

## Article

# Berriasian–Valanginian Geochronology and Carbon-Isotope Stratigraphy of the Yellow Cat Member, Cedar Mountain Formation, Eastern Utah, USA

Robert M. Joeckel <sup>1,\*</sup>, Celina A. Suarez <sup>2</sup>, Noah M. McLean <sup>3</sup>, Andreas Möller <sup>3</sup> , Gregory A. Ludvigson <sup>4</sup>, Marina B. Suarez <sup>3</sup>, James I. Kirkland <sup>5</sup> , Joseph Andrew <sup>3</sup>, Spencer Kiessling <sup>4</sup> and Garrett A. Hatzell <sup>2</sup> 

<sup>1</sup> Conservation and Survey Division, School of Natural Resources, University of Nebraska-Lincoln, Lincoln, NE 68583-0996, USA

<sup>2</sup> Department of Geosciences, University of Arkansas, Fayetteville, AR 72701, USA

<sup>3</sup> Department of Geology, University of Kansas, Lawrence, KS 66045, USA

<sup>4</sup> Kansas Geological Survey, University of Kansas, Lawrence, KS 66047, USA

<sup>5</sup> Utah Geological Survey, Salt Lake City, UT 84116, USA

\* Correspondence: rjoeckel3@unl.edu

**Abstract:** The Early Cretaceous Yellow Cat Member of the terrestrial Cedar Mountain Formation in Utah, USA, has been interpreted as a “time-rich” unit because of its dinosaur fossils, prominent paleosols, and the results of preliminary chemostratigraphic and geochronologic studies. Herein, we refine prior interpretations with: (1) a new composite C-isotope chemostratigraphic profile from the well-known Utahraptor Ridge dinosaur site, which exhibits  $\delta^{13}\text{C}$  features tentatively interpreted as the Valanginian double-peak carbon isotope excursion (the so-called “Weissert Event”) and some unnamed Berriasian features; and (2) a new cryptotephra zircon eruption age of  $135.10 \pm 0.30/0.31/0.34$  Ma ( $2\sigma$ ) derived from the CA-ID-TIMS U-Pb analyses of zircons from a paleosol cryptotephra. Our interpretations of  $\delta^{13}\text{C}$  features on our chemostratigraphic profile, in the context of our new radiometric age, are compatible with at least one prior age model for the “Weissert Event” and the most recent revision of the Cretaceous time scale. Our results also support the interpretation that the Yellow Cat Member records a significant part of Early Cretaceous time.

**Keywords:** carbon-isotope chemostratigraphy; U-Pb zircon ages; paleosol; cryptotephra; mudstone



**Citation:** Joeckel, R.M.; Suarez, C.A.; McLean, N.M.; Möller, A.; Ludvigson, G.A.; Suarez, M.B.; Kirkland, J.I.; Andrew, J.; Kiessling, S.; Hatzell, G.A. Berriasian–Valanginian Geochronology and Carbon-Isotope Stratigraphy of the Yellow Cat Member, Cedar Mountain Formation, Eastern Utah, USA. *Geosciences* **2023**, *13*, 32. <https://doi.org/10.3390/geosciences13020032>

Academic Editors: Jesus Martinez-Frias and José Manuel Castro

Received: 7 October 2022

Revised: 17 January 2023

Accepted: 23 January 2023

Published: 26 January 2023



**Copyright:** © 2023 by the authors. Licensee MDPI, Basel, Switzerland. This article is an open access article distributed under the terms and conditions of the Creative Commons Attribution (CC BY) license (<https://creativecommons.org/licenses/by/4.0/>).

## 1. Introduction

The Yellow Cat Member of the terrestrial Cedar Mountain Formation is known worldwide for its diverse fossil vertebrates, and particularly its dinosaur fossils [1,2]. It is dominated by alluvial mudrocks with prominent, stacked paleosols [2–4]. Palustrine to lacustrine sediments, including nodular to bedded carbonates (“calcretes”) are locally prominent, and fluvial sandstones are comparatively minor components [1,3,4]. Previous research carried out by some of us over more than a decade [3–7] has established the value of comprehensive stable-isotope geochemistry in the Cedar Mountain Formation, especially when coupled with radiometric dating, yet our geochronologic framework the formation is still incomplete. It is a persistent challenge to establish reliable geochronology in widely distributed continental stratigraphic sections in the absence of widespread marker beds and marine biota and under the severe constraints of exceedingly few or no observable tephtras. Our results, however, demonstrate the value of the concept of cryptotephtras [8] in challenging terrestrial sedimentary successions.

The Yellow Cat Member is particularly intriguing—and even problematic—because: (1) its depositional extent was limited to a part of southeastern Utah by ancient salt tectonics, (2) its dinosaur faunas suggest that the unit records a large part of Early Cretaceous time, (3) its well-developed Vertisol-like paleosols are likely to record long intervals of geologic time within a few meters or less of sediments [1–4], and, therefore, (4) it is thought

to be a “time-rich” unit [4]. We present a new composite  $\delta^{13}\text{C}$  chemostratigraphic profile at Utahraptor Ridge, Utah (Figure 1), where the Stikes Quarry has been excavated over a period of years for spectacular dinosaur fossils, including the remains of the eponymous dromaeosaurid *Utahraptor* [1,2]. We also provide U-Pb zircon ages from the same stratigraphic section. Earlier work identified multiple Aptian–Albian carbon-isotope excursions (CIEs) in chemostratigraphic profiles of the Cedar Mountain Formation [5,6] and demonstrated that some strata in the Yellow Cat Member are older than Aptian [3]. The present paper presents new results that verify the Berriasian–Valanginian ages of part of the Yellow Cat Member and extend the organic carbon-isotope record of the member farther back in geologic time than ever before. Some of the CIEs that we identify herein may correlate globally.

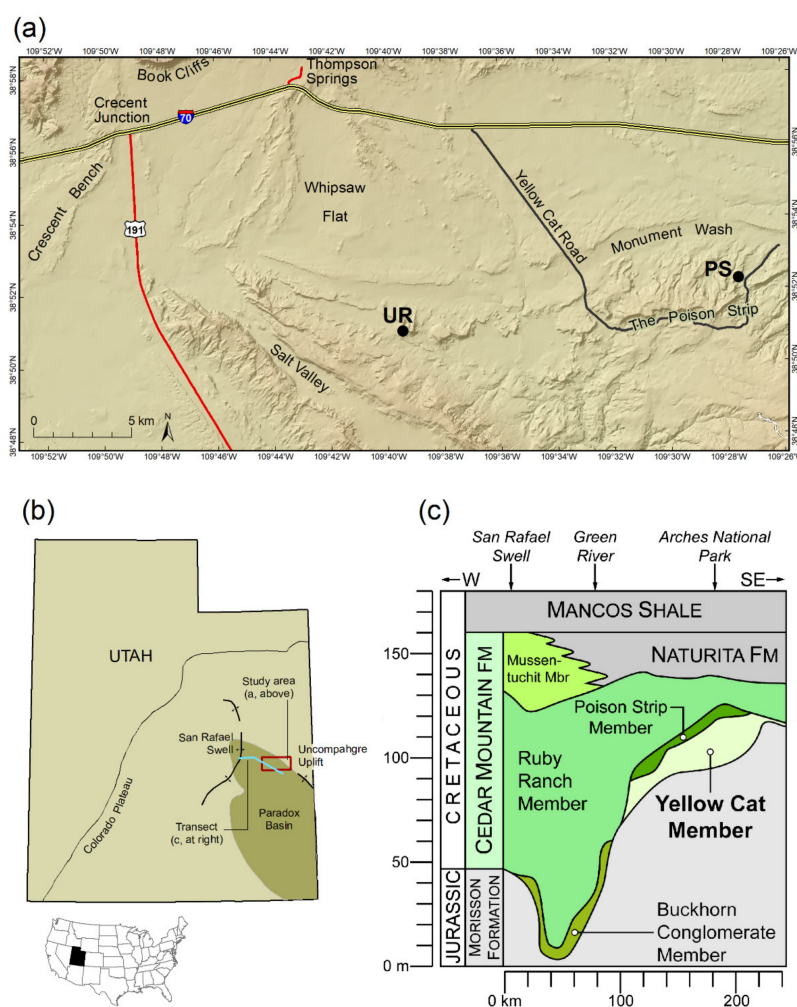


**Figure 1.** Geographic and stratigraphic setting of study site. (a) Location of Utahraptor Ridge site (UR) in Grand County, Utah, USA. The Yellow Cat Member of the Cedar Mountain Formation was previously described by Joeckel et al. [3,4] at Poison Strip (PS). (b) Location of study area identified in (a) within Utah and relative to major structural and physiographic features. (c) Simplified cross-section of Cedar Mountain Formation in southeastern Utah.

## 2. Materials and Methods

We sampled strata of the Yellow Cat Member at Utahraptor Ridge (Figures 2 and 3), a section that has been described in great detail by Kirkland et al. [2] (their figure 19), and to which we refer readers for more detail. The Yellow Cat Member at Utahraptor Ridge consists of four distinct stratigraphic intervals. A lower interval (approximately 0–3.5 m in stratigraphic height in Figure 2) consists of light gray to white, very fine to

very coarse, and pebbly sandstones. The coarse-grained, basal unit of this interval lies atop the Brushy Basin Member of the Morrison Formation (Jurassic). The thick overlying interval (approximately 3.5–26.5 m in Figure 2) is dominated by light greenish-gray to red paleosol-bearing mudstones. It also contains a few, thin intervals of sandstone and nodular carbonates (“calcretes”). A prominent “calcrete” (approximately 26.5–32 m in Figure 2) consists chiefly of large to very large nodules of fine-grained carbonate with minor interstitial mudstone. This interval is prominent and the top of it (#2 in Figures 2 and 3) is useful in local correlations. Another mudstone-dominated interval with intercalated sandstones (32 m and above in Figure 2) overlies the thick “calcrete.” The position of Stikes Quarry, an important vertebrate fossil site, is at approximately 37 m in our measured section (Figure 2: #3). There are slight discrepancies between the stratigraphic heights of units in Kirkland et al. [2] (their figure 19) and our stratigraphic section. Nevertheless, the top of the thick “calcrete” interval is readily identifiable in both their measured section and ours (Figures 2 and 3).

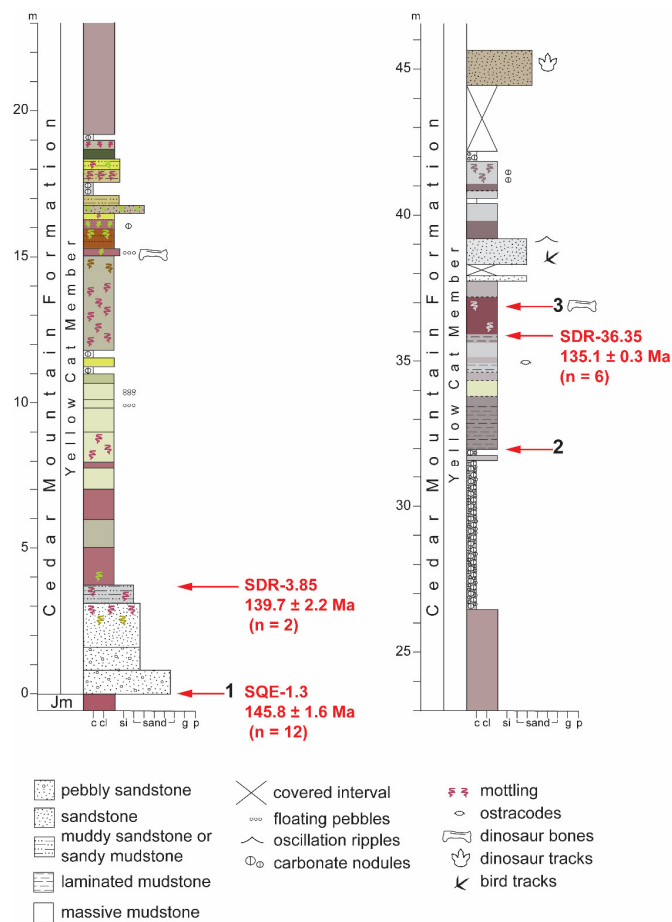


**Figure 2.** Stratigraphic section at Utahraptor Ridge. Important contacts in bold black numerals 1–3 are: (1) top of the Brushy Basin Member of the Jurassic Morrison Formation (Jm); (2) top of a thick and prominent “calcrete” or horizon of large to very large carbonate nodules, described by Kirkland et al. [2] (their figure 19); and (3) approximate position of Stikes Quarry, also described by Kirkland et al. [2] (their figure 19). Kirkland et al. [2] (their figure 19) placed the top of the “calcrete” at 30 m above the upper contact of the Morrison Formation, whereas it is placed at approximately 32 m in ours. This slight

difference probably results from local relief on stratigraphic contacts. Likewise, the position of Stikes Quarry is higher above the Morrison Formation in our section relative to that of Kirkland et al. [2] (their figure 19). Three concordia ages (red letters and numbers) derived from LA-ICP-MS zircon analyses are shown in red at their stratigraphic positions: SQE-1.3 ( $145.8 \pm 1.6$  Ma), SDR-3.85 ( $139.7 \pm 2.2$  Ma), and SDR-36.35 ( $136.1 \pm 1.2$  Ma) were reported by Joeckel et al. [3]. A newly revised high-precision CA-ID-TIMS age for SDR-36.35 is shown here. This estimated eruption age of  $135.1 \pm 0.3$  Ma is reported for the first time in this paper. Abbreviations for grain-size scale are carbonate (c), clay (cl), silt (si), granules (g), and pebbles (p); sand ticks in part of scale labeled “sand” correspond to very fine, fine, medium, coarse, and very coarse sand, from left to right. Colors in the stratigraphic column approximate rock colors in the field.

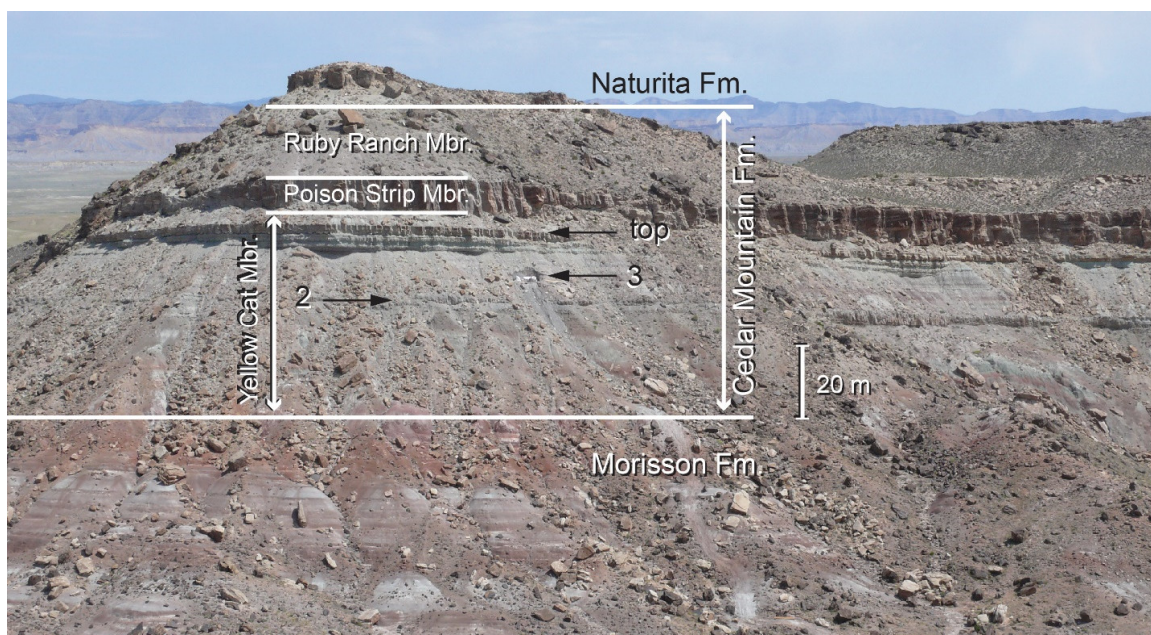


**Figure 3.** West end of Utahraptor Ridge, Utah, looking north; photograph taken approximately parallel to strike. Stratigraphic levels 2 and 3 are also identified in Figure 2. Stratigraphic level identified as “top” is the top of the stratigraphic section in Figure 2.

Our new work at Utahraptor Ridge is contextualized by prior work in the immediate area. Joeckel et al. [4] examined exceptionally good exposures of the Yellow Cat Member less than 10 km to the east at the Poison Strip site (Figure 1, “PS”). These authors demonstrated that vertical paleosol features such as filled cracks, very common small slickensides, and prominent synformal sets of very large slickensides are pervasive in massive, blocky-weathering mudstones that dominate the Yellow Cat Member at Poison Strip and other nearby outcrops. They also documented multiple instances of multigenerational paleosol crack fills that piped ancient surface sediments from on top of paleosol surfaces downward nearly to the bases of ancient soil profiles (Figure 4). Moreover, the ubiquitous large slickensides in paleosol profiles at Poison Strip evince the obliquely upward movement of clastic sediment (soil material) and carbonates by shear by ancient pedoturbation [4]. The Poison Strip exposures are nearly pristine vertical faces under an overhanging sandstone unit, but the equivalent part of the Yellow Cat Member at Utahraptor Ridge lacks such a protective overhang, is much less well-exposed, and is partially covered by talus blocks and colluvium (Figure 3). These conditions preclude making parallel, detailed observations across hundreds of meters of pristine paleosol outcrop (as at Poison Strip). Nevertheless, examinations of vertically extensive shallow trenches at Utahraptor Ridge indicate that the Yellow Cat Member there is dominated by massive mudstones with some of the same paleosol features that can be seen at Poison Strip, namely blocky weathering, carbonate

nodules, small slickensides, and color zonation reminiscent of soil horizons. Given the proximity of Utahraptor Ridge to Poison Strip and the general similarity of these paleosol features in mudstones at the two sites, we surmise that Cretaceous soil-forming processes and their climatic and hydrologic controls were very similar in both places. If ancient soils in both places experienced some degree of pedoturbation, then sediment grains, masses of soil material, soil organic carbon, and other material of different ages, compositions, and origins, would have been mixed vertically and laterally. Therefore, the successions in the Yellow Cat Member at Utahraptor Ridge and Poison Strip are unlikely to be perfectly superposed vertical successions, at least within paleosol profiles, which are approximately 0.5 to 4 m in thickness. This point is germane to interpretations of organic  $\delta^{13}\text{C}$  chemostratigraphic results and volcanogenic zircon dates made in the Discussion section of this paper.

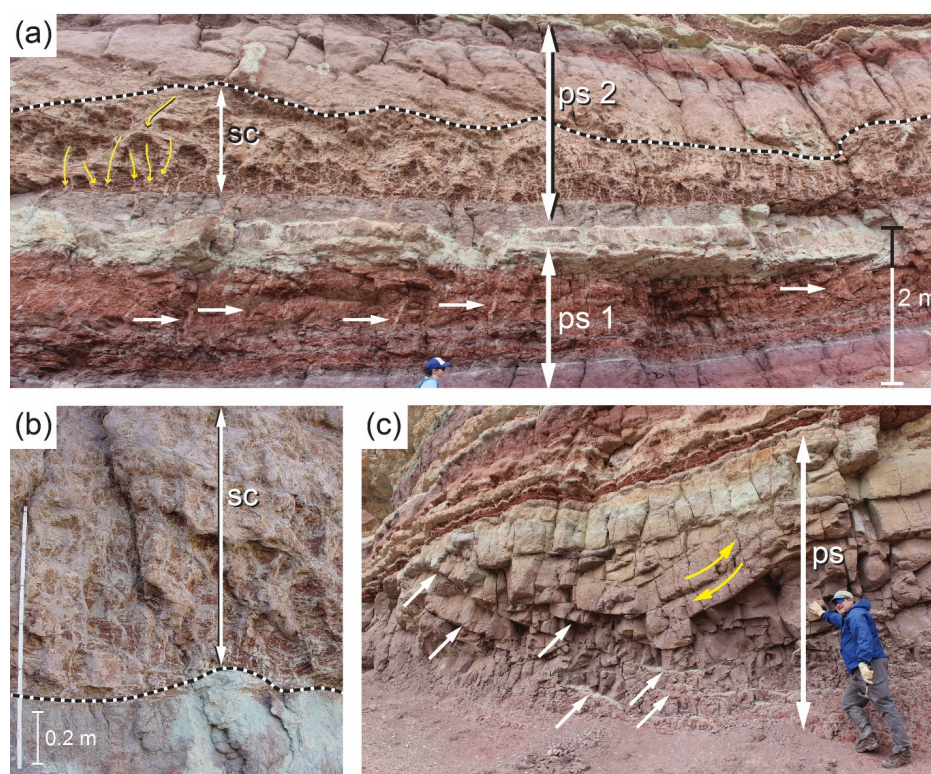


**Figure 4.** Photos illustrating paleo-Vertisol features in the Yellow Cat Member at Poison Strip, Utah (Figure 1; PS), where local conditions have maintained exceptional paleosol exposures of far greater quality than those at Utahraptor Ridge (Figure 3). (a) Two stacked paleosols (ps1, ps2); ps1 contains several carbonate-filled cracks (horizontal white arrows), and ps2 exhibits a zone of prominent, filled soil cracks (sc). Pathways of the downward translocation of sandier soil material from above into clayey soil material below are shown for selected cracks as yellow arrows at the left. (b) Closeup of soil cracks (sc) in ps2. (c) Another paleosol (ps) with prominent slickensides, identified by diagonal white arrows; general sense of shear along slickensides is shown by yellow arrows. Shear within this Early Cretaceous soil profile moved materials obliquely up and down. Features shown in these photographs suggest that perfect stratigraphic superposition (e.g., of paleosol organic matter and volcanogenic zircons) is very unlikely to exist within these paleosol profiles due to ancient pedoturbation. We propose that conditions were similar at Utahraptor Ridge during the Early Cretaceous (see text for further discussion).

Palynological results from prior research, especially when interpreted in the context of preliminary ostracode and charophyte biostratigraphy [3], very strongly suggest that the Yellow Cat Member predates the late Barremian. Thus, Joeckel et al. [3] assigned the Yellow Cat Member to the middle Berriasian to early Hauterivian stages (i.e., a range encompassing the Valanginian Stage) based on the presence of *Foraminisporis wonthaggiensis*

and *Trilobosporites* sp. cf. *T. canadensis*, and the absence of *F. asymmetricus*, *Appendicisporites* spp. and angiosperms.

### 2.1. Carbon-Isotope Analyses

We produced two new organic  $\delta^{13}\text{C}$  profiles for a stratigraphic section of the Yellow Cat Member at Utahraptor Ridge. These two profiles are combined in a composite chemostratigraphic profile, with a sample gap between the approximate stratigraphic heights of 19 to 33 m (Figure 5). This sample-gap interval spanned a section with extremely hazardous slopes that precluded collection. Chemostratigraphic samples from the Utahraptor Ridge section were collected by personnel from the University of Arkansas. These samples were sent to the University of Kansas Keck Paleoenvironmental and Environmental Stable Isotope Lab (KPESIL), where they were powdered with a mortar and pestle to generate approximately 1 g of powder. Samples were then decarbonated with 0.5 M hydrochloric acid for at least 24 h or until samples no longer reacted with fresh acid. Samples were then rinsed with deionized water by centrifugation and decanting of rinsed water until no longer acidic. Rinsed samples were dried at 50 °C and re-homogenized with a synthetic ruby mortar and pestle and stored in borosilicate vials. Raw  $\delta^{13}\text{C}$  values were obtained via high-temperature combustion with a Costech ECS 4010 Elemental analyzer connected to a continuous-flow ThermoFinnigan MAT 253 isotope ratio mass spectrometer at KPESIL. Samples were corrected to the VPDB scale using linear regression of in-house and international standards (USGS 24, IAEA 600, DORM, and IAEA C6). Calibration lines typically yield  $R^2$  values of 0.9994 or better. Multiple analyses of DORM were also used to determine the precision of 0.2‰. Organic  $\delta^{13}\text{C}$  data from Utahraptor Ridge are presented in Table 1. As is common practice in chemostratigraphic studies of sedimentary strata [3,9–11]), we employ a moving average of  $\delta^{13}\text{C}$  values in the chemostratigraphic profile derived from our data (Figure 5).

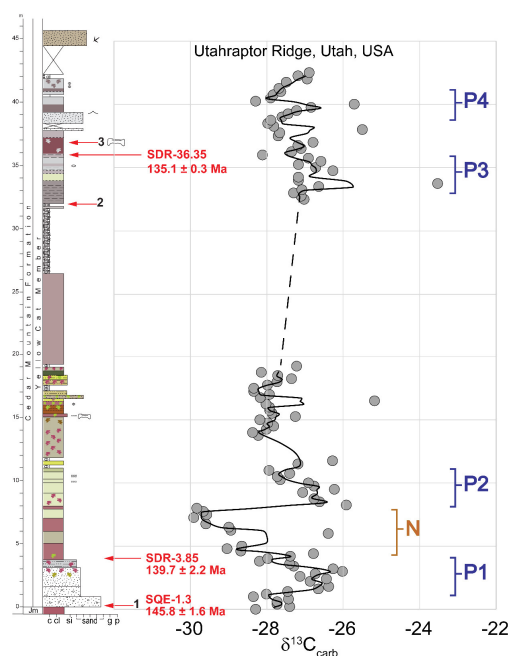


**Figure 5.** The  $\delta^{13}\text{C}$  chemostratigraphic profile (trend line is a smoothed 3-point moving average) from Yellow Cat Member, overlying Jurassic Morrison Formation (Jm) at Utahraptor Ridge. The stratigraphic position of a new high-precision eruption age of cryptotephra from sample SDR-36.35, as well as those of other published LA-ICP-MS concordia ages are shown in red; sample gap indicated by dashed line. “P” denotes positive  $\delta^{13}\text{C}$  features on the 3-point moving average curve described in text and “N” denotes a prominent negative feature. See Figure 1 and text for details. Raw data are presented in Table 1.

**Table 1.** Organic  $\delta^{13}\text{C}$  and total organic carbon (TOC%) values from sedimentary rock samples at Utahraport Ridge. Stratigraphic height refers to position in Figure 5.

Sample	Stratigraphic Height (m)	Organic $\delta^{13}\text{C}$	TOC %
SQ-0	0	−28.29	0.06
SQ-1	0.2	−27.4	0.05
SQ-2	0.4	−27.73	0.05
SQ-3	0.6	−27.73	0.05
SQ-4	0.8	−27.43	0.03
SQ-5	1	−28.35	0.04
SQ-6	1.2	−28.01	0.04
SQ-7	1.4	−27.45	0.03
SQ-8	1.6	−26.65	0.08
SQ-9	1.8	−26.38	0.04
SQ-10	2	−25.45	0.06
SQ-11	2.2	−26.86	0.08
SQ-12	2.4	−26.44	0.06
SQ-13	2.6	−27.13	0.06
SQ-14	2.8	−26.73	0.06
SQ-15	3	−26.02	0.06
SQ-16	3.2	−26.26	0.06
SQ-17	3.4	−27.29	0.06
SQ-18	3.6	−27.4	0.05
SQ-19	3.8	−28.19	0.05
SQ-20	4	−27.97	0.04
SQ-21	4.2	−27.38	0.06
SQ-22	4.4	−26.78	0.05
SQ-23	4.6	−28.68	0.09
SQ-24	4.8	−29.04	0.09
SQ-25	5	−28.65	0.08
SQ-26	6	−26.39	0.12
SQ-27	6.25	−28.94	0.08
SQ-28	6.5	−28.99	0.11
SQ-29	6.75	−29.59	0.09
SQ-31	7.25	−29.91	0.08
SQ-32	7.5	−29.57	0.1
SQ-33	7.75	−29.66	0.1
SQ-34	8	−29.83	0.09
SQ-35	8.25	−25.92	0.07
SQ-36	8.5	−26.62	0.05
SQ-37	8.75	−26.76	0.06
SQ-38	9	−27.55	0.07
SQ-39	9.25	−27.06	0.06
SQ-40	9.5	−26.23	0.06
SQ-41	9.75	−26.76	0.06
SQ-42	10	−26.91	0.06
SQ-43	10.25	−27.65	0.05
SQ-44	10.5	−27.72	0.04
SQ-45	10.75	−27.4	0.05
SQ-46	11	−27.94	0.05
SQ-48	11.5	−27.18	0.13
SQ-49	11.75	−26.28	0.16
SQ-50	13.75	−28.22	0.05
SQ-51	14	−28.37	0.04
SQ-52	14.25	−28.01	0.04
SQ-53	14.5	−27.82	0.03
SQ-54	14.75	−27.97	0.04
SQ-55	15	−28.18	0.04

Table 1. Cont.

Sample	Stratigraphic Height (m)	Organic $\delta^{13}\text{C}$	TOC %
SQ-56	15.25	−27.25	0.06
SQ-57	15.5	−27.86	0.04
SQ-58	15.75	−27.92	0.05
SQ-59	16	−27.93	0.04
SQ-60	16.25	−28.02	0.05
SQ-61	16.5	−25.18	0.05
SQ-62	16.75	−28.17	0.03
SQ-63	17	−27.93	0.04
SQ-64	17.25	−28.34	0.04
SQ-65	17.5	−28.34	0.12
SQ-66	17.75	−27.98	0.05
SQ-67	18	−27.73	0.05
SQ-68	18.25	−27.35	0.05
SQ-69	18.5	−27.71	0.06
SQ-70	18.75	−28.14	0.17
SQ-71	19	−27.54	0.14
SQ-72	19.25	−27.22	0.21
SQ-73	32.5	−27.02	0.05
SQ-74	32.75	−27.1	0.07
SQ-75	33	−27.3	0.04
SQ-76	33.25	−27.08	0.14
SQ-77	33.5	−26.64	0.05
SQ-78	33.75	−23.53	0.08
SQ-79	34	−27.17	0.09
SQ-80	34.25	−27.17	0.04
SQ-81	34.5	−15.65	0.32
SQ-82	34.75	−26.27	0.1
SQ-83	35	−26.72	0.13
SQ-84	35.25	−27.17	0.06
SQ-85	35.5	−26.58	0.09
SQ-86	35.75	−26.91	0.08
SQ-87	36	−28.11	0.19
SQ-88	36.25	−27.35	0.09
SQ-89	36.5	−27.1	0.09
SQ-90	36.75	−27.18	0.06
SQ-91	37	−26.79	0.06
SQ-92	37.25	−27.12	0.06
SQ-93	37.5	−27.7	0.05
SQ-94	37.75	−27.66	0.06
SQ-95	38	−25.5	0.05
SQ-96	38.25	−27.81	0.05
SQ-97	38.5	−27.97	0.03
SQ-98	38.75	−27.89	0.05
SQ-99	39	−27.6	0.03
SQ-100	39.25	−27.44	0.03
SQ-101	39.5	−27.22	0.03
SQ-102	38.25	−27.11	0.03
SQ-103	38.5	−26.75	0.03
SQ-104	38.75	−26.94	0.03
SQ-105	39.75	−26.84	0.06
SQ-106	40	−25.71	0.06
SQ-107	40.25	−28.29	0.25
SQ-108	40.5	−27.9	0.06
SQ-109	40.75	−27.83	0.06
SQ-110	41	−27.63	0.15
SQ-111	41.25	−27.68	0.04

Table 1. Cont.

Sample	Stratigraphic Height (m)	Organic $\delta^{13}\text{C}$	TOC %
SQ-112	41.5	−22.34	0.08
SQ-113	41.75	−27.49	0.04
SQ-114	42	−26.94	0.09
SQ-115	42.25	−27.18	0.04
SQ-116	42.5	−26.89	0.05

## 2.2. U-Pb Zircon Analyses

Zircons from sample SDR 36.35, derived from a paleosol with the potential to preserve volcanogenic zircons, were separated by standard heavy mineral separation techniques at the Isotope Geochemistry Laboratories at the University of Kansas. LA-ICPMS U-Pb data were reported from this sample in Joeckel et al. [3], with a reported concordia age of  $136.1 \pm 1.2$  Ma ( $2\sigma$ ), MSWD = 1.03. To refine this date, additional zircons were mounted and analyzed by LA-ICPMS, and then the youngest population was plucked from the grain mount for analysis by CA-ID-TIMS.

Zircons selected for Chemical Abrasion-Isotope Dilution-Thermal Ionization Mass Spectrometry (CA-ID-TIMS) were ultrasonicated and cleaned in 6 M HCl on the hotplate before being ‘annealed’ at 900 °C for 60 h, then ‘leached’ for 12 h in 29 M HF at 210 °C [12] in Teflon microcapsules inside Parr dissolution vessels. Zircon grains were then removed from the microcapsules, ultrasonicated, rinsed in 7M HNO<sub>3</sub>, 6 M HCl, and MQ water, and loaded back in microcapsules with ~50  $\mu\text{L}$  of 29 M HF and ~10  $\mu\text{L}$  of EARTHTIME ET535 <sup>205</sup>Pb–<sup>233</sup>U–<sup>235</sup>U tracer solution [13,14] for dissolution at 210 °C for 48 h. Dissolved samples were then dried down in the microcapsules and redissolved in ~50  $\mu\text{L}$  of 6 M HCl at 180 °C for 12 h inside the Parr dissolution vessels. The resulting solutions were again dried down, redissolved in ~50  $\mu\text{L}$  of 3 M HCl, and then U and Pb were separated from other elements using 50  $\mu\text{L}$  anion exchange columns with AG1X8 resin using a procedure modified after Krogh [15]. The combined U and Pb separates were dried down with ~1  $\mu\text{L}$  of 0.001 M H<sub>3</sub>PO<sub>4</sub>.

The U plus Pb samples were later mixed with ~2  $\mu\text{L}$  of silica gel activator [16] and loaded onto degassed zone-refined Re filaments for analysis on the Isotopx Phoenix TIMS at the University of Kansas. A peak-hopping method was used to measure Pb isotopes on the Daly ion counting system behind a WARP filter, and Pb isotopic fractionation was corrected using a factor of  $0.16 \pm 0.04$  ( $2\sigma$ ) %/amu (based on long-term measurements of the NBS 981 Pb reference material). U was measured as UO<sub>2</sub> using a static Faraday method, with a correction for the <sup>233</sup>U<sup>18</sup>O<sup>16</sup>O isotopologue’s interference on <sup>235</sup>U<sup>16</sup>O<sup>16</sup>O assuming an <sup>18</sup>O/<sup>16</sup>O of 0.00205 inside of the Tripoli software; isotopic fractionation correction for U was determined using the tracer’s <sup>233</sup>U/<sup>235</sup>U and an assumed zircon <sup>238</sup>U/<sup>235</sup>U of  $137.818 \pm 0.045$  ( $2\sigma$ ) [17]. U-Pb data reduction was performed in the ET Redux software [18,19], assuming all Pb comes from laboratory blank and correcting for initial <sup>230</sup>Th/<sup>238</sup>U disequilibrium using a conservative estimated Th/U<sub>magma</sub> of  $3.5 \pm 2.0$  ( $2\sigma$ ). U-Pb ID-TIMS data are presented in Table 2.

**Table 2.** U-Pb Chemical Abrasion-Isotope Dilution-Thermal Ionization Mass Spectrometry (CA-ID-TIMS) for zircons from sample SDR 36.35 at Utahraport Ridge.

SDR	Dates (Ma)		Composition					Isotopic Ratios					Correlation Coefficients						
	$^{206}\text{Pb}/^{238}\text{U}$ <Th> <sup>a</sup>	$\pm 2\sigma$ abs	$^{207}\text{Pb}/^{235}\text{U}$ <sup>b</sup>	$\pm 2\sigma$ abs	$^{207}\text{Pb}/^{206}\text{Pb}$ <sup>b</sup>	$\pm 2\sigma$ abs	% disc <sup>c</sup>	Th/ U <sup>d</sup>	Pbc (pg) <sup>e</sup>	Pb*/ Pbc <sup>f</sup>	$^{206}\text{Pb}/^{204}\text{Pb}$ <sup>g</sup>	$^{206}\text{Pb}/^{238}\text{U}$ <Th> <sup>ha</sup>	$\pm 2\sigma$ %	$^{207}\text{Pb}/^{235}\text{U}$ <sup>h</sup>	$\pm 2\sigma$ %	$^{207}\text{Pb}/^{206}\text{Pb}$ <sup>h</sup>	$\pm 2\sigma$ %	$^{206}\text{Pb}/^{238}\text{U}$ <Th>- $^{207}\text{Pb}/^{235}\text{U}$	Fraction
Fraction 2021-142	135.32	0.12	135.32	0.53	137.1	8.8	1.38	0.18	0.67	19.96	1380	0.021214	0.091	0.14256	0.42	0.04880	0.37	0.554	2021-142
Zircon 56	135.67	0.11	136.18	0.87	147	15	7.59	0.30	0.70	10.09	686	0.021270	0.086	0.14353	0.68	0.04900	0.63	0.622	56
2021-048	135.28	0.30	134.7	2.7	127	48	-6.35	0.27	1.66	3.77	269	0.021207	0.22	0.1419	2.2	0.04859	2.0	0.536	2021-048
2021-132	135.06	0.76	134.2	2.9	120	48	-12.57	0.51	0.80	5.79	380	0.021171	0.57	0.1413	2.3	0.04844	2.0	0.554	2021-132
2021-142	135.32	0.12	135.32	0.53	137.1	8.8	1.38	0.18	0.67	19.96	1380	0.021214	0.091	0.14256	0.42	0.04880	0.37	0.554	2021-142
2021-207	135.23	0.34	134.9	2.7	131	46	-3.26	0.21	1.57	4.34	312	0.021199	0.25	0.1421	2.1	0.04867	2.0	0.668	2021-207
2021-316	136.38	0.29	135.7	1.8	125	31	-9.36	0.61	7.74	5.58	357	0.021382	0.22	0.1429	1.4	0.04854	1.3	0.469	2021-316

<sup>a</sup> Corrected for initial Th/U disequilibrium using radiogenic 208Pb and Th/U[magma] = 3.5. <sup>b</sup> Isotopic dates calculated using  $\lambda_{238} = 1.55125 \times 10^{-10}$  (Jaffey et al. 1971) and  $\lambda_{235} = 9.8485 \times 10^{-10}$  (Jaffey et al. 1971). <sup>c</sup> % discordance =  $100 - (100 \times (206\text{Pb}/238\text{U date}) / (207\text{Pb}/206\text{Pb date}))$ . <sup>d</sup> Th contents calculated from radiogenic 208Pb and 230Th-corrected 206Pb/238U date of the sample, assuming concordance between U-Pb Th-Pb systems. <sup>e</sup> Total mass of common Pb. <sup>f</sup> Ratio of radiogenic Pb (including 208Pb) to common Pb. <sup>g</sup> Measured ratio corrected for fractionation and spike contribution only. <sup>h</sup> Measured ratios corrected for fractionation, tracer, and blank.

### 3. Results

#### 3.1. Carbon-Isotope Analyses

Organic carbon  $\delta^{13}\text{C}$  values from the composite chemostratigraphic profile at Utahrap-tor Ridge range from a minimum of about  $-30\%$  VPDB up to about  $-23.5\%$  VPDB. Our chemostratigraphic profile (Figure 5) shows data points for individual carbon isotope analyses along with a smoothed 3-point moving average trend line that we use to determine the approximate magnitude of  $\delta^{13}\text{C}$  shifts. The dashed line in Figure 5 represents the sample gap and it merely connects  $\delta^{13}\text{C}$  values from immediately below and above the gap. The long-term trend through the whole carbon isotope profile shows slightly increasing  $\delta^{13}\text{C}$  values upward through the section (Figure 5).

Carbon isotope  $\delta^{13}\text{C}$  values of about  $-28\%$  VPDB appear to characterize baseline values at the bottom (0 to 1.5 m), middle (approximately 13 to 19 m), and near the top of the profile (approximately 33, 36, 38, and 40 m). Critically, these baseline intervals bracket other intervals with well-defined chemostratigraphic structures (Figure 5). Apparent positive carbon-isotope features exist at approximate stratigraphic heights of: (1) 1 to 4 m, with a shift with a magnitude of about 2 per mil (Figure 5: P1); (2) 9 to 12 m, with a shift with a magnitude of about 1.5 per mil (Figure 5: P2); (3) 34 to 36 m, with a shift with a magnitude of about 1 per mil (Figure 5: P3); and 39 to 41 m, with a shift with a magnitude of 1 per mil (Figure 5, P4). One apparent negative carbon-isotope feature is present at a stratigraphic height of 4 to 8 m and it has a shift with a magnitude of about 2 per mil (Figure 5: N). We also note that the P3 and P4 intervals include chemostratigraphic samples with yet even higher “outlier”  $\delta^{13}\text{C}$  values. Carbon isotope values of  $-23.53\%$  and  $-25.71\%$  were produced from samples at stratigraphic heights of 33.75 m and 40 m respectively. Those sample positions coincide with the peak  $\delta^{13}\text{C}$  values of P3 and P4, and might actually be more indicative of the full magnitude of these CIEs at Utahrap-tor Ridge.

#### 3.2. U-Pb Zircon Analyses

Six zircons analyzed by CA-ID-TIMS yield concordant  $^{230}\text{Th}$ -corrected U-Pb dates between 136.4 Ma and 135 Ma. The youngest four form a tight cluster around 135.3 Ma, in good agreement with the LA-ICPMS U-Pb concordia date of  $136.1 \pm 1.2$  Ma ( $2\sigma$ ) reported in Joeckel et al. [3]. We interpret the scatter in zircon ages well outside their uncertainties as evidence of prolonged zircon crystallization or incorporation of zircons in this sample from slightly older magmatic systems. The youngest age represented what we interpret as our best estimate of the zircons’ eruption age and the maximum depositional age of the sample. To estimate the minimum of the zircons’ age spread, we use the Bayesian algorithm presented by Keller et al. [20]. This approach avoids artificially reducing the age uncertainty when evaluating a weighted mean of the youngest zircons up to an arbitrary and ambiguous cutoff age. As illustrated in Figure 6, the uncertainty is  $\pm 0.30/0.31/0.34$  Ma ( $2\sigma$ ). The uncertainty is given in the form X/Y/Z, where X includes analytical sources of uncertainty, Y additionally includes uncertainty in calibration of the ET535 isotopic tracer, and Z includes analytical, tracer, and decay constant uncertainty contributions.

We consider our volcanogenic zircon samples to represent cryptotephra. Our usage of the term cryptotephra [8], in this case refers, to the technical approach of laboratory separation of microscopic fragments from volcanic tephra deposits that are contained within sedimentary units (in the present case, paleosol-bearing mudstones) that show no visible evidence of volcanic ash deposition in the field. The processing sequence for Quaternary cryptotephra [8] differs from ours in that microscopic volcanic glass shards are concentrated from mudstone paleosol samples in the laboratory for the purpose of chemical fingerprinting of known well-dated Quaternary tephra deposits. In the case of our Early Cretaceous cryptotephra, microscopic zircon crystals are concentrated in the laboratory for the purpose of LA-ICP-MS U-Pb screening of large zircon populations to identify the Maximum Depositional Age (MDA) age cluster. Given that LA-ICP-MS ages have a 2% range of uncertainty, higher-precision CA-ID-TIMS U-Pb analyses of zircon crystals from the MDA age cluster are required to refine age models with appropriate sub-million-year uncertainties.

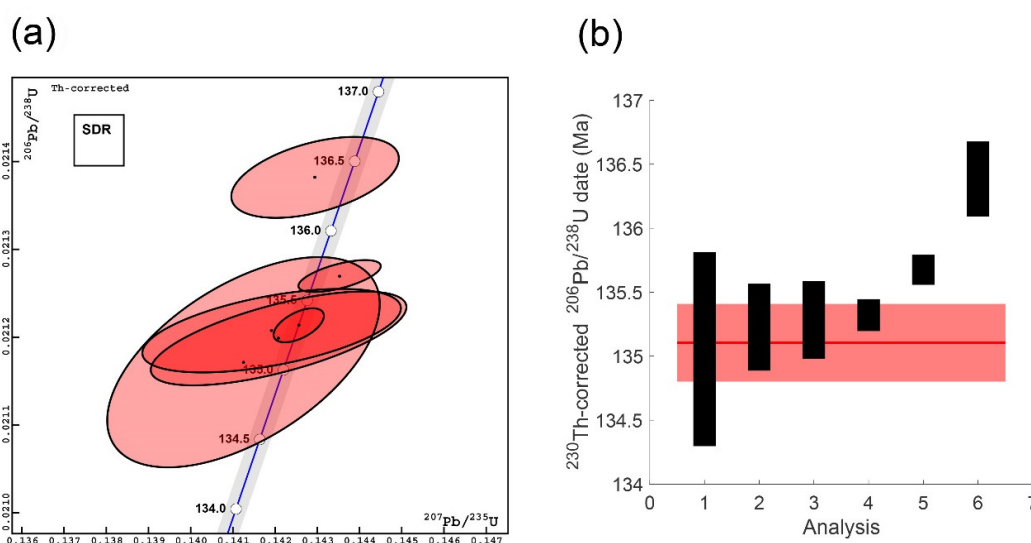


**Figure 6.** U-Pb CA-ID-TIMS data for sample SDR 36.35. (a) Plot showing  $2\sigma$  uncertainty ellipses for the six zircon analyses in Table 2. The blue line is concordia, the gray shaded region is the  $2\sigma$  uncertainty defined by the  $^{238}\text{U}$  and  $^{235}\text{U}$  decay constant uncertainties, and all data have been corrected for initial  $^{230}\text{Th}$  disequilibrium. (b) Age-rank plot of analyzed zircon dates. Black boxes illustrate  $\pm 2\sigma$  analytical uncertainties, and the red-shaded region is the calculated best estimate of the eruption and maximum depositional age using the algorithm of Keller et al. [20]. See Table 2 for data.

#### 4. Discussion

C-isotope chemostratigraphy from Utahrapator Ridge is tentatively correlated with other pre-Hauterivian chemostratigraphic records around the world in Figure 7. Given the eruption age of  $135.1 \pm 0.3$  Ma of a cryptotephra from 36.35 m above the contact between the underlying Morrison Formation and the Cedar Mountain Formation contact, we interpret the C-isotope record from 32.5 to 42.5 m as Valanginian s and the C-isotope record from 0 to 19.25 m as Berriasian. We specify CIEs in the chemostratigraphic profile at Utahrapator Ridge as comparatively short-term departures from, and subsequent returns to, the long-term baseline  $\delta^{13}\text{C}$  values. Thus, a positive CIE exhibits an underlying rising limb of increasing  $\delta^{13}\text{C}$  values culminating in a maximum  $\delta^{13}\text{C}$  value, with an overlying falling limb of decreasing values returning to the long-term baseline  $\delta^{13}\text{C}$  values. Conversely, a negative CIE has an underlying falling limb culminating in a minimum  $\delta^{13}\text{C}$  value, overlain by a rising limb and an eventual return to the long-term baseline  $\delta^{13}\text{C}$  values.

In support of our analysis of Berriasian chemostratigraphy, we note the seminal identification of two minor positive CIEs that were reported from pelagic marine carbonates from the Berriasian stratotype by Emmanuel and Renard [21] from the Vocontian basin of southeast France (Figure 7). The magnitude of the positive carbon-isotope shifts described by these authors is  $+0.32$  and  $+0.37$  per mil, respectively. A more recent analysis of marine Berriasian chemostratigraphy at the La Chambotte section on the Jura Platform by Morales et al. [22] showed a similar structure, but with much larger carbon-isotope shifts of about 2 per mil. Given our age constraints derived from volcanogenic zircons, we correlate the Berriasian positive carbon isotope chemostratigraphic features described by Emmanuel and Renard [21] to the  $+2.3$  per mil positive  $\delta^{13}\text{C}$  shift at approximately 3 m in stratigraphic height at Utahrapator Ridge (within P1 in Figure 5) and to the  $+4.0$  per mil positive  $\delta^{13}\text{C}$  shift at 8.25 m (within P2 in Figure 5). The magnitudes of the positive carbon isotope shifts in our continental organic  $\delta^{13}\text{C}$  record from Utahrapator Ridge are much greater than the CIEs to which we correlate them in the marine carbonate record. Notwithstanding, it is common for terrestrial  $\delta^{13}\text{C}$  chemostratigraphic records to exhibit magnitudes that exceed those of correlative marine records by factors of two or more (Table 3) [4–6,11,23–41]. The causes of such frequently observed differences between correlative terrestrial and marine  $\delta^{13}\text{C}$  records have not been fully explored. Notwithstanding, cogent observations can be brought

to bear on the matter, such as the realization that terrestrial records directly capture temporal shifts in the  $\delta^{13}\text{C}$  composition of atmospheric  $\text{CO}_2$ , while correlated marine records are likely to be buffered by a marine dissolved inorganic carbon reservoir that exceeds that of the atmosphere by 50 to 60 times [20]. Therefore, potential leads and lags—the mixing times of the atmospheric and marine carbon reservoirs, which differ by orders of magnitude—are important considerations in the recording of C-cycle perturbations in the sedimentary record. Emmanuel and Renard [21] interpreted the Berriasian  $\delta^{13}\text{C}$  chemostratigraphy in their section as related to sequence stratigraphic and sea-level changes.

**Table 3.** Comparison of magnitudes of published marine and terrestrial records of well-known Cretaceous and Paleogene carbon-isotope excursions (CIEs), exemplifying comparative differences in the magnitudes. See text for further explanation.

Publication	Carbon-Isotope Excursion (CIE) Events	Marine CIE Magnitude	Terrestrial CIE Magnitude
Bains [23]	Paleocene–Eocene Thermal Maximum	2.5 per mil 0.0 to 2.5‰	5.5 to 8 per mil −15.5 to 8.5‰
Gröcke et al. [24]	Albian–Cenomanian OAE 1d	1.5 per mil 0.2 to 1.6‰	3 per mil −26 to −23‰
Gröcke and Joeckel [25]	Albian–Cenomanian OAE 1d	—	4 per mil −26.4 to −22.6‰
Richey et al. [26]	Albian–Cenomanian OAE 1d	—	3 per mil −26 to −23‰
Andrzejewski et al. [27]	Albian–Cenomanian OAE 1d	—	5 per mil −29 to −24‰
Ross et al. [11]	Albian C15 segment	0.5 per mil 2.0 to 2.5‰	4 per mil −27 to −23‰
Ludvigson et al. [5]	Aptian OAE 1a, 1b	2 per mil 2.0 to 4.0‰	3 per mil −6 to −3‰
Ludvigson et al. [6]	Aptian OAE 1a, 1b	2 per mil 2.0 to 4.0‰	3 per mil −6 to −3‰
Channell et al. [38]	Valanginian CIE	1.5 per mil 1.5 to 3.0‰	—
Erba et al. [41]	Valanginian CIE	1.5 per mil 1.5 to 3.0‰	—
Celestino et al. [28]	Valanginian CIE	2 per mil 1.0 to 3.0‰	—
Cavalheiro et al. [29]	Valanginian CIE	1 per mil −31 to −30‰	—
Robinson & Hesselbo [30]	Valanginian CIE	1.5 per mil 1.5 to 3.0‰	4 per mil −25 to −21‰
Gröcke et al. [31]	Valanginian CIE	1.5 per mil 1.5 to 3.0‰	4 per mil −24 to −20‰
Joeckel et al. (this report)	Valanginian CIE	2 per mil 1.0 to 3.0‰	2 per mil −28 to −26‰
Emmanuel and Reynard [21]	Early Berriasian CIEs	1 per mil 0.5 to 1.5‰	—
Morales et al. (2013)	Early Berriasian CIEs	2 per mil 0.0 to 2.0‰	—
Joeckel et al. (this report)	Early Berriasian CIEs	—	4 per mil −30 to −26‰

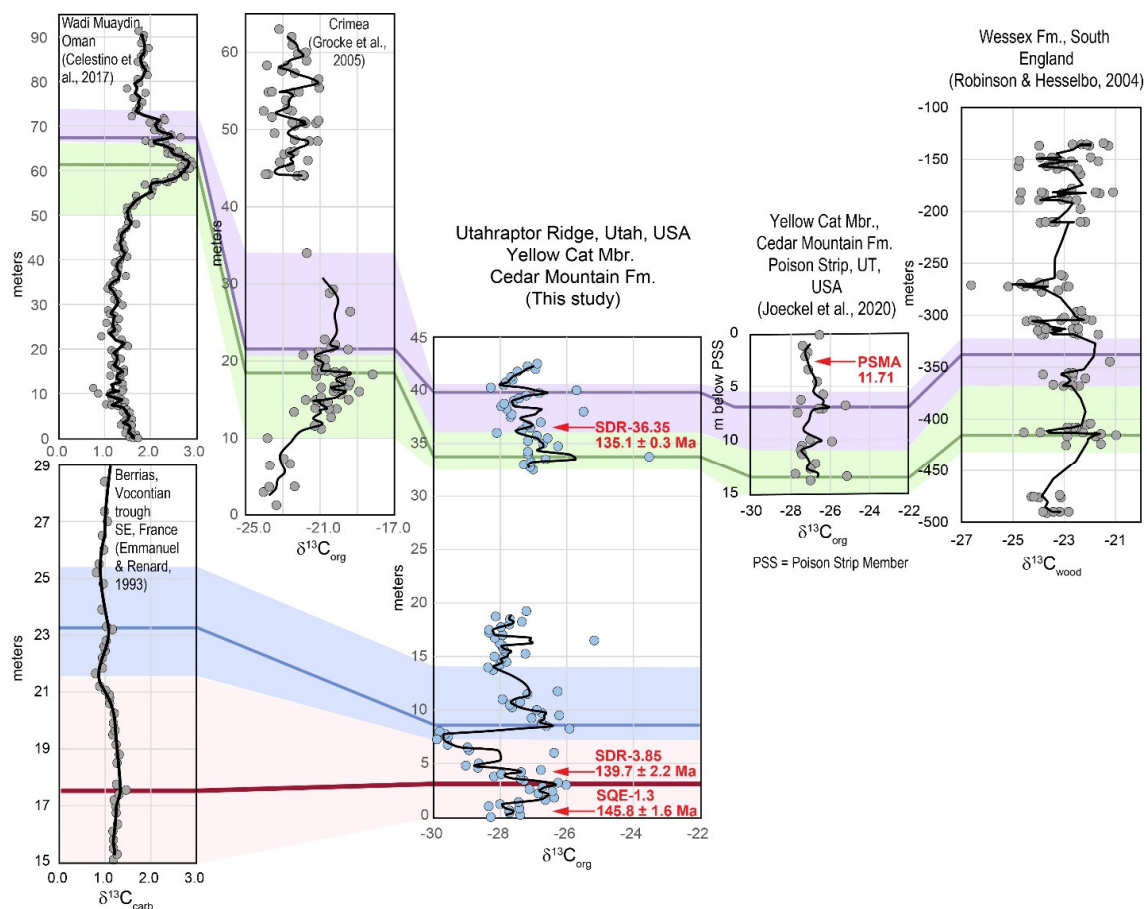


**Figure 7.** Comparison of new composite chemostratigraphic profile from Utahraptor Ridge with profiles from nearby Poison Strip, Utah (see Figure 1), as well as Oman, France, Crimea, and England [21,28,30,31]. The correlation of the Valanginian carbon isotope excursion by Robinson and Hesselbo [30] has been here further subdivided into the upper and lower  $\delta^{13}\text{C}$  peaks.

If correctly correlated, ours is one of only a few terrestrial organic  $\delta^{13}\text{C}$  records of Berriasian age and it indicates potentially significant C-cycle perturbations of unknown origin. We note that positive feature P1 at Utahraptor Ridge (Figure 5) qualifies as a CIE because it has both rising and falling limbs, whereas positive feature P2 (Figure 5) is a very abrupt positive shift relative to underlying  $\delta^{13}\text{C}$  values and has no rising limb per se. A future effort in finer-scale sampling frequency could determine whether there are intermediate values in the profile at Utahraptor Ridge. Morales et al. [22] (their figure 5) effectively report the same phenomenon at the approximate 25 m level in the Berriasian La Chambotte section on the Jura Platform in eastern France, a chemostratigraphic profile, which also shows an abrupt increase in  $\delta^{13}\text{C}$  values between two adjacent samples. Furthermore, there is an uncanny resemblance between the Berriasian  $\delta^{13}\text{C}$  profiles at La Chambotte of Morales et al. [22] and the part of our composite  $\delta^{13}\text{C}$  profile that we propose to be Berriasian strata at Utahraptor Ridge.

Positive CIEs with possible magnitudes of as much as +3.6 per mil at 33.75 m in stratigraphic height and of possibly as much as +2.3 per mil slightly below 40 m in our chemostratigraphic profile at Utahraptor Ridge (Figure 5: P3, P4). Furthermore, the overall configuration of our chemostratigraphic profile between approximately 33.75 and 40 m (Figure 5) is strongly reminiscent of the “double-peak” positive C-isotope excursion in the Valangian observed in many marine carbonate records and called the “Weissert Event” or “Weissert Episode” by some authors [31–46] (Figure 7). In the chemostratigraphic profile presented in Figure 5, we interpret feature P3 as the lower of the two peaks and P4 as the upper one. The Valangian positive CIE records the first of several major perturbations

of the global carbon cycle during the Cretaceous Period [31–34]. Although it has been identified chiefly in marine carbonate strata, the “Weissert Event” was first identified in continental strata nearly two decades ago [30]. Recently, Joeckel et al. [3] proposed evidence for this event in a chemostratigraphic profile of the Yellow Cat Member at Poison Strip (Figures 1 and 4), but our recent results presented herein add further weight to this idea. The magnitude of the positive CIEs at the “Weissert Event,” where it is firmly identified in terrestrial records, are  $\sim +3$  per mil from the pre-excursion background for the first peak and  $\sim +1.5$  per mil for the second peak isotope excursion in these carbonate records. This C-isotope trend is also seen in continental records of coal and charcoal [31], but at a much higher magnitude (+5.9 per mil and +2.41 per mil); it is noteworthy that the data from Utahraptor Ridge are consistent with this trend. Furthermore, the SDR-36.35 mudstone paleosol sample at Utahraptor Ridge is one of two (the other being sample PSMA-11.71) that produced large  $n$  clusters of Valanginian zircon grains from the LA-ICP-MS U-Pb data reported by Joeckel et al. [3]. The Maximum Depositional Age (MDA;  $136.1 \pm 1.24$  Ma) reported from this cluster of zircons in SDR-36.35 is a close approximation to some published ages for the Valanginian positive CIE or “Weissert Event” [47] and marked this sample as a likely paleosol cryptotephra. Our high-precision eruption age of  $135.1 \pm 0.3$  Ma for sample SDR-36.35 is a close match to the recently estimated age of the Weissert Event at 135 to 134 Ma [47]. Testing our hypothesis that the “Weissert Event” can be identified in the Yellow Cat Member will require more work. If our hypothesis is correct, however, we are the first identification and in situ age assessment of the WE in terrestrial sediments in North America.

We have already compared, by way of sedimentologic context, the Yellow Cat Member at Utahraptor Ridge with the same unit at the nearby Poison Strip, Utah. This comparison strongly suggests that ancient pedoturbation occurred at both sites and materials atop and within paleosol profiles—including those we sampled for organic  $\delta^{13}\text{C}$  analyses and volcanogenic zircons—were mixed vertically and laterally to some degree. It is very unlikely, then, that there is a perfect vertical superposition of sediments (i.e., paleosol materials) of slightly different ages through multiple paleosol profiles approximately 0.5 to 4 m in thickness. Accordingly, neither individual organic  $\delta^{13}\text{C}$  values nor volcanogenic zircons derived from analyses of either stratigraphic section may be in the exact stratigraphic positions in which they were originally accumulated. In this scenario, the detailed structure of a resulting chemostratigraphic profile would be modified relative to an equivalent hypothetical sedimentary succession with perfect vertical superposition. Isotopic signatures of carbon-cycle change would thus be “smeared” across paleosol-bearing intervals because soil organic matter of slightly different ages in our samples may not have been directly superimposed at decimeter-to-meter scales. To some extent, our use of a three-point moving average trend line mitigates the potential impacts of vertical translocation due to ancient pedoturbation. Such effects would affect only the details of the curve at scales of a few meters or less, and not the overall trend of  $\delta^{13}\text{C}$  values. We observe that a similar approach in pelagic marine carbonates mitigates the effects of the “bioturbation window” through centimeter-to-decimeter stratigraphic intervals.

In view of such potential complications, we are inclined to draw particular attention to our reported organic  $\delta^{13}\text{C}$  values greater than  $-26\text{‰}$  in our sections (Figure 5). Those values are within intervals that express positive  $\delta^{13}\text{C}$  excursions in successive samples at the decimeter scale in the line representing our three-point moving average (Figure 5). Thus, even though they do not lie on that curve, they may still represent  $\delta^{13}\text{C}$  peak values within CIEs. The fact remains that at both Poison Strip locality [3,4] and Utahraptor Ridge, there are significant, positive  $\delta^{13}\text{C}$  excursions that are expressed at the meter-to-decimeter scale. Moreover, a recent, but as-yet unpublished, chemostratigraphic study of the Yellow Cat Member in eastern Utah independently reports other probable records of the Valanginian double-peak  $\delta^{13}\text{C}$  excursion or “Weissert Event” [48].

Comparisons of our interpretive record of the Valanginian CIE at Utahraptor Ridge with other published  $\delta^{13}\text{C}$  profiles widely accepted to record the event indicates that there

are local or regional differences in its expression. We observe: (1) that 13 correlated  $\delta^{13}\text{C}$  profiles from the Pacific to Europe compiled by Duchamp-Alphonse et al. [46] show such differences, (2) many records of the Valanginian CIE display two discrete lower and upper  $\delta^{13}\text{C}$  peaks (the record at Poison Strip begins at the position of this lower peak, and (3) the  $\delta^{13}\text{C}$  values in the lower peak are nearly always higher than in the upper peak.

## 5. Conclusions

This paper continues a longstanding line of inquiry into the stable-isotope chemostratigraphy and geochronology of the Cedar Mountain Formation e.g., [3,5–7]. The lower part of a distinctive double-peak positive carbon-isotope excursion in a composite  $\delta^{13}\text{C}$  chemostratigraphic profile of the Yellow Cat Member from Utahrapator Ridge, Utah is directly associated with a cryptotephra zircon eruption age of  $135.10 \pm 0.30/0.31/0.34$  Ma ( $2\sigma$ ) derived from the U-Pb CA-ID-TIMS analyses of paleosol zircons. These geochronological and chemostratigraphic results are consistent with the absolute age model of Channell et al. [38] for the Valanginian positive carbon-isotope excursion or so-called “Weissert Event” in a succession of marine carbonates in Europe. Moreover, our results and our interpretation of a Valanginian double-peak C-isotope excursion are compatible with the most recent placements of not only the “Weissert Event” (135–134 Ma), but also the Berriasian–Valanginian boundary (137 Ma) and the Valanginian–Hauterivian boundary (132 Ma) [47].

Our work also identifies important avenues for future research. High-precision U-Pb geochronologic analyses can be used to test the hypothesis that the “Weissert Event” is recorded in the study area. Furthermore, the probable Berriasian  $\delta^{13}\text{C}$  features we have identified in our composite  $\delta^{13}\text{C}$  chemostratigraphic profile from Utahrapator Ridge almost certainly have broader significance, and they too should be scrutinized in future research.

**Author Contributions:** R.M.J., C.A.S., N.M.M., A.M. and G.A.L.: compilation and writing. R.M.J., C.A.S., A.M., G.A.L., M.B.S., J.I.K. and G.A.H.: field work. C.A.S., M.B.S., N.M.M., A.M., M.B.S., J.A. and S.K.: analyses. All authors have read and agreed to the published version of the manuscript.

**Funding:** This research received no external funding.

**Data Availability Statement:** The data presented in this study are available in this article.

**Acknowledgments:** We thank Bruce Barnett for supervising the C-isotope analyses at Keck Paleoenvironmental and Environmental Stable Isotope Laboratory at the University of Kansas and Allie Ryan for sample processing. We also thank three anonymous reviewers whose suggestions greatly improved this paper. Editorial office assistants for their patient editorial efforts and encouragement. Julius Csotonyi graciously provided an excellent illustration for our graphical abstract.

**Conflicts of Interest:** The authors declare no conflict of interest.

## References

1. Kirkland, J.I.; Simpson, E.L.; DeBlieux, D.D.; Madsen, S.K.; Bogner, E.; Tibert, N.E. Depositional constraints on the Lower Cretaceous Stikes Quarry dinosaur site: Upper Yellow Cat Member, Cedar Mountain Formation, Utah. *Palaios* **2016**, *31*, 421–439. [[CrossRef](#)]
2. Kirkland, J.; Suarez, M.; Suarez, C.; Hunt-Foster, R. The Lower Cretaceous in east-central Utah—The Cedar Mountain Formation and its bounding strata. *Geol. Intermount. West* **2016**, *3*, 101–228. [[CrossRef](#)]
3. Joeckel, R.M.; Ludvigson, G.A.; Möller, A.; Hotton, C.L.; Suarez, M.B.; Suarez, C.A.; Sames, B.; Kirkland, J.I.; Hendrix, B. Chronostratigraphy and terrestrial palaeoclimatology of Berriasian–Hauterivian strata of the Cedar Mountain Formation, Utah, USA. In *Cretaceous Climate Events and Short-Term Sea-Level Changes*; Geological Society, Special Publications 498; Wagemich, M., Hart, M.B., Sames, B., Yilmaz, I.O., Eds.; Geological Society of London: London, UK, 2020; pp. 75–100.
4. Joeckel, R.M.; Ludvigson, G.A.; Kirkland, J.I. Lower Cretaceous paleo-Vertisols and sedimentary interrelationships in stacked alluvial sequences, Utah, USA. *Sediment. Geol.* **2017**, *361*, 1–24. [[CrossRef](#)]
5. Ludvigson, G.A.; Joeckel, R.M.; Gonzalez, L.A.; Gulbranson, E.L.; Rasbury, E.T.; Hunt, G.J.; Kirkland, J.I.; Madsen, S. Correlation of Aptian–Albian carbon isotope excursions in continental strata of the Cretaceous foreland basin of eastern Utah. *J. Sediment. Res.* **2010**, *80*, 955–974. [[CrossRef](#)]
6. Ludvigson, G.A.; Joeckel, R.M.; Murphy, L.R.; Stockli, D.F.; González, L.A.; Suarez, C.A.; Kirkland, J.I.; Al-Suwaidi, A. The emerging terrestrial record of Aptian–Albian global change. *Cretac. Res.* **2015**, *56*, 1–24. [[CrossRef](#)]

7. Suarez, M.B.; Knight, J.A.; Godet, A.; Ludvigson, G.A.; Snell, K.E.; Murphy, L.; Kirkland, J.I. Multiproxy strategy for determining palaeoclimate parameters in the Ruby Ranch Member of the Cedar Mountain Formation. In *Stable Isotope Studies of the Water Cycle and Terrestrial Environments*; Geological Society, Special Publications 507; Bojar, A.-V., Pelc, A., Lécuyer, C., Eds.; Geological Society of London: London, UK, 2020; pp. 313–334.
8. Davies, S.M. Cryptotephra: The revolution in correlation and precision dating. *J. Quat. Sci.* **2015**, *30*, 114–130. [[CrossRef](#)]
9. Herrle, J.O.; Kössler, P.; Bollman, J. Palaeoceanographic differences of early Late Aptian black shale events in the Vocontian Basin (SE France). *Palaeogeogr. Palaeoclimatol. Palaeoecol.* **2010**, *297*, 367–376. [[CrossRef](#)]
10. Bornemann, A.; Mutterlose, J. Calcareous nannofossil and  $\delta^{13}\text{C}$  records from the Early Cretaceous of the western Atlantic Ocean: Evidence for enhanced fertilization across the Berriasian–Valanginian transition. *Palaios* **2008**, *23*, 821–832. [[CrossRef](#)]
11. Ross, J.B.; Ludvigson, G.A.; Möller, A.; Gonzalez, L.; Walker, J.D. Stable isotope paleohydrology and chemostratigraphy of the Albian Wayan Formation from the wedge-top depozone, North American Western Interior Basin. *Sci. China Earth Sci.* **2017**, *60*, 44–57. [[CrossRef](#)]
12. Mattinson, J.M. Zircon U-Pb chemical abrasion (“CA-TIMS”) method: Combined annealing and multi-step partial dissolution analysis for improved precision and accuracy of ages. *Chem. Geol.* **2005**, *220*, 47–66. [[CrossRef](#)]
13. Condon, D.J.; Schoene, B.; McLean, N.M.; Bowring, S.A.; Parrish, R.R. Metrology and traceability of U-Pb isotope dilution geochronology (EARTHTIME tracer calibration Part I). *Geochim. Cosmochim. Acta* **2015**, *164*, 464–480. [[CrossRef](#)]
14. McLean, N.M.; Condon, D.J.; Schoene, B.; Bowring, S.A. Evaluating uncertainties in the calibration of isotopic reference materials and multi-element isotopic tracers (EARTHTIME Tracer Calibration Part II). *Geochim. Cosmochim. Acta* **2015**, *164*, 481–501. [[CrossRef](#)]
15. Krogh, T.E. A low-contamination method for hydrothermal decomposition of zircon and extraction of U and Pb for isotopic age determinations. *Geochim. Cosmochim. Acta* **1973**, *37*, 485–494. [[CrossRef](#)]
16. Gerstenberger, H.; Haase, G. A highly effective emitter substance for mass spectrometric Pb isotope ratio determinations. *Chem. Geol.* **1997**, *136*, 309–312. [[CrossRef](#)]
17. Hiess, J.; Condon, D.J.; McLean, N.; Noble, S.R.  $^{238}\text{U}/^{235}\text{U}$  systematics in terrestrial uranium-bearing minerals. *Science* **2012**, *335*, 1610–1614. [[CrossRef](#)] [[PubMed](#)]
18. McLean, N.M.; Bowring, J.F.; Bowring, S.A. An algorithm for U-Pb isotope dilution data reduction and uncertainty propagation. *Geochem. Geophys. Geosyst.* **2011**, *12*, Q0AA18. [[CrossRef](#)]
19. Bowring, J.F.; McLean, N.M.; Bowring, S.A. Engineering cyber infrastructure for U-Pb geochronology: Tripoli and U-Pb Redux. *Geochem. Geophys. Geosyst.* **2011**, *12*, Q0AA19. [[CrossRef](#)]
20. Keller, C.B.; Schoene, B.; Samperton, K.M. A stochastic sampling approach to zircon eruption age interpretation. *Geochem. Perspec. Lett.* **2018**, *8*, 31–35. [[CrossRef](#)]
21. Emmanuel, L.; Renard, M. Carbonate geochemistry (Mn,  $\delta^{13}\text{C}$ ,  $\delta^{18}\text{O}$ ) of the Late Tithonian—Berriasian pelagic limestones of the Vocontian trough (SE France). *Bull. Cent. Recher. Expl. Prod. Elf-Aquitaine* **1993**, *17*, 205–221.
22. Morales, C.; Gardin, S.; Cshnyder, J.; Spangenberg, J.; Arnaud-Vanneau, A.; Arnaud, H.; Adatte, T.; Föllmi, K.B. Berriaian and early early Valanginian environmental change along a transect from the Jura Platform to the Vocotian Basin. *Sedimentology* **2007**, *60*, 36–63. [[CrossRef](#)]
23. Bains, S.; Norris, R.D.; Corfield, R.; Bowen, G.J.; Gingerich, P.D.; Koch, P.L. Marine-terrestrial linkages at the Paleocene-Eocene boundary. In *Causes and Consequences of Globally Warm Climates of the Early Paleogene*; Geological Society of America Special Paper, 369; Wing, S., Gingerich, P.D., Schmitz, B., Thomas, E., Eds.; Geological Society of America: Boulder, CO, USA, 2003; pp. 1–9.
24. Gröcke, D.R.; Ludvigson, G.A.; Witzke, B.L.; Robinson, S.A.; Joeckel, R.M.; Ufnar, D.F.; Ravn, R.L. Recognizing the Albian-Cenomanian (OAE1d) sequence boundary using plant carbon isotopes: Dakota Formation, Western Interior Basin, USA. *Geology* **2006**, *34*, 193–196. [[CrossRef](#)]
25. Gröcke, D.R.; Joeckel, R.M. A Stratigraphic test of the terrestrial carbon-isotope record of the latest Albian OAE from the Dakota Formation, Nebraska. In *Field Trip 2: Fluvial-Estuarine Deposition in the Mid-Cretaceous Dakota Formation, Kansas and Nebraska*; Kansas Geological Survey, Open-File Report no. 2008-2; University of Kansas: Lawrence, KS, USA, 2002; pp. 24–30.
26. Richey, J.D.; Upchurch, G.R.; Montañez, I.P.; Lomax, B.H.; Suarez, M.B.; Crout, N.M.J.; Joeckel, R.M.; Ludvigson, G.A.; Smith, J.J. Changes in  $\text{CO}_2$  during the Ocean Anoxic Event 1d indicate similarities to other carbon cycle perturbations. *Earth Planet. Sci. Lett.* **2018**, *491*, 172–182. [[CrossRef](#)]
27. Andrzejewski, K.A.; Layzell, A.L.; Ludvigson, G.A.; Joeckel, R.M.; Möller, A.; Mandel, R.D. Unique insights to the Cretaceous OAE1d, Mid-Cenomanian Event, and OAE2 from long-line drillcores along the eastern cratonic margin of the Western Interior Basin. In Proceedings of the 2022 Perkins-Rosen Conference, Gulf Coast Section SEPM (Society for Sedimentary Geology), Houston, TX, USA, 5–7 December 2022.
28. Celestino, R.; Wohlwend, S.; Rehakova, D.; Weissert, H. Carbon isotope stratigraphy, biostratigraphy and sedimentology of the Upper Jurassic—Lower Cretaceous Rayda Formation, Central Oman Mountains. *Newsl. Stratigr.* **2017**, *50*, 91–109. [[CrossRef](#)]
29. Cavalheiro, L.; Wagner, T.; Steinig, S.; Bottini, C.; Dummann, W.; Esegbue, O.; Gambacorta, G.; Giraldo-Gómez, V.; Farnsworth, A.; Flögel, S.; et al. Impact of global cooling on Early Cretaceous high  $\text{pCO}_2$  world during the Weissert Event. *Nat. Commun.* **2021**, *12*, 5411. [[CrossRef](#)]
30. Robinson, S.A.; Hesselbo, S.P. Fossil-wood carbon-isotope stratigraphy of the non-marine Wealden Group (Lower Cretaceous, southern England). *J. Geol. Soc.* **2004**, *161*, 133–145. [[CrossRef](#)]

31. Gröcke, D.R.; Price, G.D.; Robinson, S.A.; Baraboshkin, E.Y.; Mutterlose, J.; Ruffell, A.H. The Upper Valanginian (Early Cretaceous) positive carbon-isotope event recorded in terrestrial plants. *Earth Planet. Sci. Lett.* **2005**, *240*, 495–509. [[CrossRef](#)]
32. Saltzman, M.R.; Thomas, E. Carbon isotope stratigraphy. In *The Geologic Time Scale 2012*; Gradstein, F.M., Ogg, J.G., Schmitz, M., Ogg, G., Eds.; Elsevier: Amsterdam, The Netherlands, 2012; pp. 207–232.
33. Schlanger, S.; Jenkyns, H. Cretaceous anoxic events: Causes and consequences. *Geol. Mijnb.* **1976**, *55*, 179–184.
34. Weissert, H. C-isotope stratigraphy, a monitor of paleoenvironmental change: A case study from the early Cretaceous. *Surv. Geophys.* **1989**, *10*, 1–61. [[CrossRef](#)]
35. Jenkyns, H.C. Geochemistry of oceanic anoxic events. *Geochem. Geophys. Geosyst.* **2010**, *11*, Q03004. [[CrossRef](#)]
36. Föllmi, K.B. Early Cretaceous life, climate and anoxia. *Cretac. Res.* **2012**, *35*, 230–257. [[CrossRef](#)]
37. Lini, A.; Weissert, H.; Erba, E. The Valanginian carbon isotope event: A first episode of greenhouse climate conditions during the Cretaceous. *Terra Nova* **1992**, *4*, 374–384. [[CrossRef](#)]
38. Channell, J.E.T.; Erba, E.; Lini, A. Magnetostratigraphic calibration of the Late Valanginian carbon isotope event in pelagic limestones from northern Italy and Switzerland. *Earth Planet. Sci. Lett.* **1993**, *118*, 145–166. [[CrossRef](#)]
39. Weissert, H.; Lini, A.; Föllmi, K.B.; Kuhn, O. Correlation of Early Cretaceous carbon isotope stratigraphy and platform drowning events: A possible link? *Palaeogeogr. Palaeoclimatol. Palaeoecol.* **1998**, *137*, 189–203. [[CrossRef](#)]
40. Föllmi, K.B.; Weissert, H.; Bisping, M.; Funk, H.P. Phosphogenesis, carbon-isotope stratigraphy, and carbonate-platform evolution along the Lower Cretaceous northern Tethyan margin. *Geol. Soc. Am. Bull.* **1994**, *106*, 729–746. [[CrossRef](#)]
41. Erba, E.; Bartolini, A.; Larson, R.L. Valanginian Weissert oceanic anoxic event. *Geology* **2004**, *32*, 149–152. [[CrossRef](#)]
42. Charbonnier, G.; Boulila, S.; Gardin, S.; Duchamp-Alphonse, S.; Adatte, T.; Spangenberg, J.E.; Föllmi, K.B.; Colin, C.; Galbrun, B. Astronomical Calibration of the Valanginian “Weissert” Episode: The Orpierre Marl–Limestone Succession (Vocontian Basin, Southeastern France). In *STRATI 2013*; Rocha, R., Pais, J., Kullberg, J.C., Finney, S., Eds.; Springer Geology: Cham, Switzerland, 2014; pp. 175–179.
43. Martinez, M.; DeConinck, J.-F.; Pellenard, P.; Riquier, L.; Company, M.; Reboulet, S.; Moiroud, M. Astrochronology of the Valanginian–Hauterivian stages (Early Cretaceous): Chronological relationships between the Paraná–Etendeka large igneous province and the Weissert and the Faraoni events. *Glob. Planet. Change* **2015**, *121*, 158–173. [[CrossRef](#)]
44. Nunn, E.V.; Price, G.D.; Gröcke, D.R.; Baraboshkin, E.Y.; Leng, M.J.; Hart, M.B. The Valanginian positive carbon isotope event in Arctic Russia: Evidence from terrestrial and marine isotope records and implications for global carbon cycling. *Cretac. Res.* **2010**, *31*, 577–592. [[CrossRef](#)]
45. Meissner, P.; Mutterlose, J.; Bodin, S. Latitudinal temperature trends in the northern hemisphere during the Early Cretaceous (Valanginian–Hauterivian). *Palaeogeogr. Palaeoclimatol. Palaeoecol.* **2015**, *424*, 17–39. [[CrossRef](#)]
46. Duchamp-Alphonse, S.; Gardin, S.; Fiet, N.; Bartolini, A.; Blamart, D.; Pagel, M. Fertilization of the northwestern Tethys (Vocotian basin, SE France) during the Valanginian carbon isotope perturbation: Evidence from calcareous nannofossils and trace element data. *Palaeogeogr. Palaeoclimatol. Palaeoecol.* **2007**, *243*, 132–151. [[CrossRef](#)]
47. Gale, A.S.; Mutterlose, J.; Batenburg, S.; Gradstein, F.M.; Agterberg, F.P.; Ogg, J.G. Chapter 27—The Cretaceous Period. In *Geologic Time Scale 2020*; Gradstein, F.M., Ogg, J.G., Schmitz, M.D., Ogg, G.M., Eds.; Elsevier: Amsterdam, The Netherlands, 2020; pp. 1023–1086.
48. Forster, C. Evaluation of Carbon Isotopic Chemostratigraphy of the Cedar Mountain Formation of Utah. Master’s Thesis, University of Arkansas, Fayetteville, AR, USA, 2022.

**Disclaimer/Publisher’s Note:** The statements, opinions and data contained in all publications are solely those of the individual author(s) and contributor(s) and not of MDPI and/or the editor(s). MDPI and/or the editor(s) disclaim responsibility for any injury to people or property resulting from any ideas, methods, instructions or products referred to in the content.